Ceramics International xxx (xxxx) xxx

Contents lists available at ScienceDirect

Ceramics International

journal homepage: www.elsevier.com/locate/ceramint

Synergistic enhancement of mechanical and superconducting performance in YBCO/Ag composite through one-pot synthesis and fiber-based densification

Matheus P. Brambilla [a], Edimar A.S. Duran [a], Alfonso Pulgar [a], Maycon Motta [b], Lucas B.S. da Silva [c], Durval Rodrigues Jr [c], Vasily S. Stolyarov [d], Rodolfo Izquierdo [a], Rafael Zadorosny [a,*]

[a] Physics and Chemistry Department, São Paulo State University (Unesp), School of Engineering, Campus Ilha Solteira, Ilha Solteira, São Paulo, Brazil
[b] Departamento de Física, Universidade Federal de São Carlos, 13565-905, São Carlos, SP, Brazil
[c] Lorena School of Engineering, University of São Paulo (USP), Lorena, São Paulo, Brazil
[d] Moscow Center for Advanced Studies, 123592, Moscow, Russia

ARTICLE INFO

Keywords:
$YBa_2Cu_3O_{7-\delta}$ (YBCO)
Solution blow spinning
High-temperature superconductors
Silver incorporation
Mechanical strengthening
Energy materials

ABSTRACT

The practical application of high-temperature superconductors (HTSCs) such as $YBa_2Cu_3O_{7-\delta}$ (YBCO) is critically hindered by their intrinsic brittleness, which compromises structural integrity. To overcome this limitation, this work introduces a synergistic strategy combining Ag incorporation, one-pot synthesis, and fiber-stacking densification. YBCO/Ag composite fibers were fabricated via Solution Blow Spinning (SBS), pressed into pellets, and systematically compared with pellet-shaped samples obtained from conventionally compacted one-pot synthesized YBCO/Ag powders. The fiber-based route yielded a denser, plate-like microstructure, leading to a remarkable 125% enhancement in Vickers hardness for the optimal 5 wt% Ag composition relative to the powder-based reference. This composition also exhibited the highest critical current density (J_c), which is attributed to a balance between Ag-induced microstructural refinement, favoring flux pinning, and the preservation of intergranular Josephson coupling. At higher silver concentrations, the increased fraction of metallic normal regions weakened the intergranular connectivity and degraded the superconducting performance. Overall, the combination of homogeneous silver incorporation via one-pot synthesis and fiber-based processing establishes a promising route for producing mechanically robust HTSC components with enhanced multifunctional performance under demanding operating conditions.

1. Introduction

High-temperature superconductors (HTSCs) have continued to attract growing research interest (see Fig. 1), particularly since the landmark discovery of the ceramic compound $YBa_2Cu_3O_{7-\delta}$ (YBCO) in 1987 [1]. The main reason is that this material exhibited a superconducting transition temperature (T_c) of 93 K, well above the boiling point of liquid nitrogen (77 K) and unprecedented at that time [1]. This breakthrough demonstrated that liquid nitrogen could be potentially used as an economical cryogenic coolant, making HTSC-based applications significantly more feasible compared with those requiring conventional low-temperature superconductors. In fact, this breakthrough not only transformed the fundamental understanding of superconductivity in cuprate materials but also catalyzed sustained growth in both the volume and impact of research on lossless current-transport devices and energy-storage systems based on HTSCs over the last decade (see Fig. 1a) [1,2].

On the other hand, although the promising superconducting properties of YBCO are widely recognized, the material presents significant structural limitations that inhibit its processing and integration into devices. Its layered crystalline structure, dominated by the CuO_2 planes responsible for the superconductivity, results in strong anisotropy and intrinsic brittleness [3–6].

Furthermore, the short coherence length of YBCO, on the order of only a few nanometers, makes the material extremely sensitive to structural defects, discontinuities, and poor inter-grain connectivity. These limitations directly degrade key properties such as the critical current density (J_c) and compromise its mechanical performance, particularly in applications that demand structural robustness and stability under intense magnetic fields [2,7].

To overcome the restrictions mentioned above, the addition of metallic elements such as Ag has become a widely employed strategy — primarily investigated using traditional solid-state synthesis routes

* Corresponding author.
E-mail addresses: matheus.p.brambilla@unesp.br (M.P. Brambilla), rafael.zadorosny@unesp.br (R. Zadorosny).

https://doi.org/10.1016/j.ceramint.2026.05.161
Received 18 February 2026; Received in revised form 8 May 2026; Accepted 11 May 2026
Available online 14 May 2026

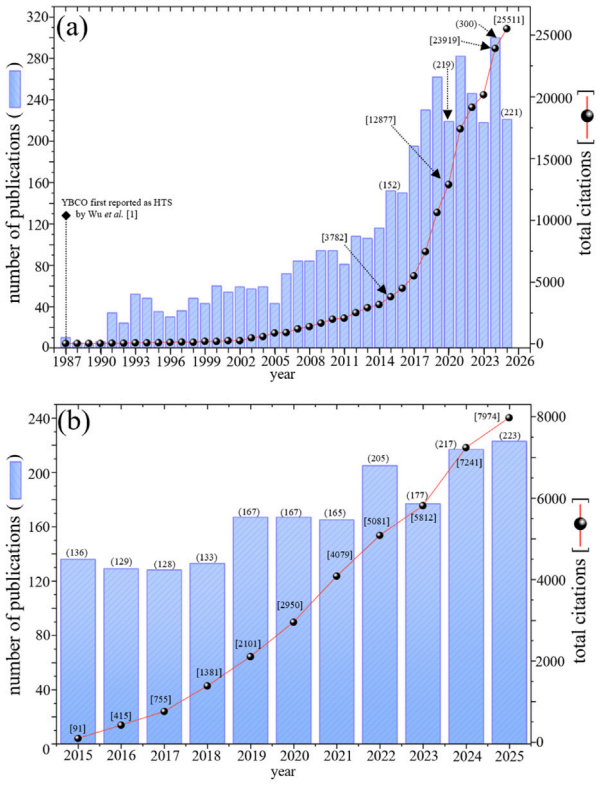

Fig. 1. (a) Annual number of publications and total citations on superconductors and their applications in lossless current-transport devices and energy-storage systems from 1987 to 2025, and (b) on superconductors with a focus on mechanical properties from 2015 to 2025. The data was extracted from the Web of Science database.

— to enhance the structural properties of YBCO [8]. Silver acts as a reinforcing agent, promoting better grain compaction, reducing porosity, and increasing mechanical strength [9–13]. This enhancement is attributed to the ability of Ag particles to relax residual stresses from the anisotropic expansion of individual grains and to provide increased resistance to crack propagation by pinning the advancing crack [6], in addition to enhancing current transport by reducing potential barriers at grain boundaries [10,12,14–18].

Recent advances in YBCO/Ag systems have demonstrated that silver incorporation can go beyond microstructural refinement, directly influencing crystallographic texture and superconducting performance. For instance, Zhao et al. [19] reported the formation of a $YBa_2Cu_{3-x}Ag_xO_{7-\delta}$ (YBCAO) solid-solution phase, which acts as a crystallographic template and promotes preferential grain orientation, leading to a 3.9-fold increase in J_c. This behavior highlights the role of Ag not only as a structural additive but also as an active agent in microstructural organization. Similarly, Zhang et al. [20] demonstrated that advanced processing routes such as additive manufacturing combined with top-seeded melt growth can produce quasi-single-crystal YBCO structures with critical current densities approaching 10^4 A cm^{-2} at 77 K. In parallel, emerging one-pot and self-assembly-based strategies have enabled precise control over hierarchical microstructure, opening new pathways to tailor superconducting properties [21].

Despite its effectiveness, the solid-state route is limited by poor control over silver dispersion and homogeneity [11,13]. Additionally, these methods struggle to minimize the formation of secondary phases. Moreover, most of these advanced strategies rely on complex processing routes, which may limit scalability and microstructural versatility. In particular, the combined effects of silver addition and alternative densification strategies in chemically synthesized YBCO systems remain insufficiently explored.

In contrast, chemical routes have emerged as promising alternatives, offering greater control over the microstructure and potentially leading to materials with enhanced uniformity and mechanical strength. Among these, one-pot synthesis has been shown to produce high-quality YBCO samples with improved superconducting properties while offering a simpler and more sustainable alternative to conventional methods [22,23].

Leveraging the high-quality homogeneous solution obtained from these chemical routes, materials structuring techniques like Solution Blow Spinning (SBS) have been employed to fabricate YBCO in the form of fibrous mats [23]. While pure YBCO fibers are known for their mechanical fragility, the SBS method has also been successfully extended to produce YBCO/Ag composite fibers [24]. In this context, the combination of chemical synthesis with fibrous structuring and controlled densification represents a promising yet still underexplored strategy. This capability underscores the potential of combining chemical synthesis with advanced structuring techniques to refine the fabrication of superconducting ceramics.

Currently, progress in the field of superconductor mechanical properties is rapidly accelerating. Fig. 1b shows statistics on the number of documents on superconductors focusing on mechanical properties over the last 10 years. As briefly outlined, the timespan from 2015 to 2025 provided abundant contributions. Concurrently, Fig. 1b also shows that, starting in 2015, the annual citation count remained consistently high; there was a notable linear increase in total citations, culminating in the current annual growth rate of 14.8% in 2024, even though 2025. This trend points toward growing interest in research on this topic.

For all these reasons, this work aims to address these gaps by investigating the influence of silver addition on the superconducting and mechanical properties of YBCO synthesized via the one-pot route [22]. In particular, we used the SBS technique to produce ceramic fibers, which were subsequently stacked and pressed into layered pellets. The results from these layered pellets were compared with those from samples made by conventional densification of granular material synthesized via the same one-pot route. This combined approach enables a direct comparison between different microstructural organizations and densification pathways, providing new insights into the interplay between processing, microstructure, and functional performance.

This article is structured as follows. Section 2 details the material synthesis and characterization techniques. Section 3 presents and discusses the results, focusing on the mechanical and superconducting behavior of samples produced with different silver concentrations and densification methodologies. Finally, Section 4 provides the conclusions.

2. Experimental

2.1. Synthesis and sample preparation

YBCO samples containing 0.5, 5, and 20 wt% silver were synthesized via an one-pot chemical route, adapted from [24], to yield a total of 2 g of final material. The precursor reagents were yttrium acetate hydrate [$Y(CH_3CO_2)_3{\cdot}xH_2O$] (0.7995 g, 99.9%), barium acetate [$Ba(CH_3CO_2)_2$] (1.5491 g, 99%), and copper acetate monohydrate [$Cu(CH_3CO_2)_2{\cdot}H_2O$] (1.8163 g, 99%). For the Ag-incorporated samples, silver acetate [$Ag(CH_3CO_2)$] (0.01548 g, 0.15552 g, and 0.62023 g for 0.5, 5, and 20 wt% silver, respectively, 99%) was also added. The acetates were dissolved in a solvent mixture of propionic acid (12 wt%), methanol (61.5 wt%), ammonium hydroxide (25.5 wt%) and finally was added poly(vinyl pyrrolidone) (PVP, Mw = 1,300,000 g/mol) to the solution at a 5:1 (acetates:PVP) weight ratio, to obtain a PVP concentration in solution of 6 wt% and the mixture was stirred for 24 h, with the Becker hermetically closed.

The viscosity of the precursor solution was measured immediately after stirring using a Cannon-Fenske 200 viscometer at room temperature (25 °C). Subsequently, the solution was divided into two batches. The first was reserved for Solution Blow Spinning (SBS). The second was heated at 200 °C (3 °C/min) for 3 h to evaporate the solvents, yielding a precursor powder after being scraped from the beaker, ground, and placed in a crucible.

The SBS process was conducted by placing the precursor solution in a hypodermic syringe connected to the SBS system, which was operated at 50 °C to prevent blockages. An injection rate of 60 μL/min and an airflow pressure of 1 bar were used. The resulting nanofibers were collected on a fixed target positioned 80 cm from the injector nozzle.

Both precursor materials, the nanofiber mats produced via SBS and the ground powder, underwent a multi-step heat treatment. The first step consisted of calcination at 600 °C, with a heating rate of 2 °C/min for 3 h, to eliminate organic matter. For the powder-route samples, this calcination step was repeated after an intermediate grinding stage to enhance homogeneity.

The final and critical stage, the sintering under oxygen flow, was essential to promote the formation of the superconducting YBCO phase. The process was carried out in a tubular furnace following the thermal profile described below: heating from room temperature to 820 °C at a rate of 2 °C/min, with oxygen flow introduced at 450 °C; holding at 820 °C for 14 h; then increasing the temperature at 1 °C/min up to 925 °C (895 °C for Ag-containing samples [24]) and maintaining it for 1 h. Cooling was performed at 1 °C/min down to 725 °C and held for 6 h, followed by a further decrease at 3 °C/min to 450 °C, where the samples were maintained for 24 h. Finally, the oxygen flow was stopped, and the furnace was allowed to cool down naturally to room temperature.

After phase formation, pellets (5 mm diameter, 2.5 mm height, ≈0.2 g) were produced by three consecutive uniaxial pressings at 5.9 MPa, each with a dwell time of 60 s. Pellets made from stacked nanofiber mats were denoted with the suffix 'F' (e.g., YBCOF), while those made from the ground powder were denoted with the suffix 'P' (e.g., YBCO-Ag5-P, i.e. YAg5P).

Subsequently, all pellets were sintered at their respective phase formation temperatures (925 °C for the pure samples and 895 °C for the Ag-added samples) for an additional 3 h to promote grain growth. In total, four sample types were produced: YBCOF, YAg5F, YBCOP, and YAg5P. For each composition, three specimens were prepared for different characterizations: magnetic measurements, spectroscopic analyses, and Vickers hardness testing.

The pellets used for Vickers hardness measurements were polished on the surface to be evaluated. Initially, a flat surface was obtained by sequential grinding using SiC papers underwater lubrication with grit sizes of 600, 800, 1200, and 2000. Subsequently, polishing was performed using alumina suspensions with particle sizes of 1 μm, 0.3 μm, and 0.05 μm. Finally, the samples were ultrasonically cleaned in pure acetone.

2.2. Characterization

Phase identification of the synthesized samples was performed by X-ray diffraction (XRD). The analysis used Cu K_α radiation ($\lambda = 1.5418$ Å), with the 2θ angle scanned from 20° to 60° at a rate of 2°/min. The average crystallite size was estimated from XRD peak broadening using the Scherrer equation:

$$D = \frac{K\lambda}{\beta \cos\theta} \tag{1}$$

where D is the crystallite size, K is the shape factor (taken as 0.9), λ is the X-ray wavelength (CuKα, $\lambda = 1.5406$ Å), β is the full width at half maximum (FWHM) of the diffraction peak, and θ is the Bragg angle.

The FWHM values were obtained by Gaussian fitting using the deconvolution function implemented in commercial software. The crystallite size was determined from the (hkl) reflections associated with the most intense peaks in the diffractogram, with 2θ values at 22.88° (003), 23.21° (100), 32.62° (013), 32.88° (103), 38.55° (005), 38.71° (113), 40.42° (113), 46.76° (020)/(006), 47.56° (200), 58.31° (116), and 58.83° (123), in the 20–60° range. These peaks correspond to the YBCOF reference sample, and the crystallite size was calculated as the average of these measurements. Instrumental broadening was not subtracted; thus, the reported values should be considered as apparent crystallite sizes.

The microstructure of fractured pellet surfaces was observed using scanning electron microscopy (SEM) to investigate sample morphology and elemental distribution. Energy-dispersive X-ray spectroscopy (EDS) was coupled with SEM to analyze the phases formed and to map the dispersion of silver within the YBCO matrix.

Vickers hardness (H_v) was evaluated on the polished surfaces of the pellets using a Shimadzu HMV microhardness tester. The measurements were conducted by applying a load of 2.942 N for a dwell time of 15 s. For each sample, an average of 13 indentations was systematically made across the surface to ensure statistical relevance. The resulting indentation diagonals were measured with an accuracy of ±0.1 μm, and the data were subsequently analyzed using MATLAB.

The superconducting properties were characterized using a Physical Property Measurement System (PPMS from Quantum Design) with the magnetic field applied parallel to the longitudinal section of the parallelepiped (orthogonal to the cylinder axis). Temperature-dependent DC magnetization ($M - T$) curves were measured to determine the superconducting critical temperature (T_c). For the Zero-Field-Cooled (ZFC) protocol, samples were cooled from 110 K to 5 K in a zero-field environment. A field of 30 Oe was then applied, and magnetization was recorded upon warming. In the sequence, the temperature was increased again maintaining the same applied magnetic field, in a Field-Cooling (FC) protocol, and magnetization was recorded while cooling.

For critical current density (J_c) evaluation, the cylindrical pellets were first cut into small rectangular prisms. Magnetic hysteresis loops ($M - H$) were then measured on these samples at 4, 2 K and 77 K. From the width of the hysteresis loops ($\Delta M = M_{\text{down}} - M_{\text{up}}$), the J_c was calculated using the Bean model [25,26].

$$J_c = \frac{20\Delta M}{a\left(1 - \frac{a}{3b}\right)} \tag{2}$$

where ΔM is expressed in emu/cm^3, a and b are the cross-sectional dimensions of the sample in cm ($a < b$), yielding J_c in A/cm^2.

3. Results and discussions

To evaluate the combined effects of silver addition and shaping methodology (powder vs. fibers), four initial samples were prepared: YBCOP, YAg5P, YBCOF, and YAg5F. The hardness distribution of the samples was simulated using colorimetric maps generated from a mesh of Vickers indentations on the pellet surfaces in four directions (North, South, East, and West), as illustrated in Fig. 2(a). Preliminary hardness results revealed a significant increase for the fiber-formed samples compared to those obtained by powder compaction, particularly in the presence of 5 wt% Ag, as shown in Fig. 2(b). Based on this promising behavior, the study was expanded to include two additional fiber-based formulations, YAg0.5F (0.5 wt% Ag) and YAg20F (20 wt% Ag), in order to investigate the influence of both lower and higher silver concentrations. This approach enabled a systematic evaluation of whether the mechanical response followed a linear trend, reached an optimal reinforcement condition, or exhibited saturation effects.

Notably, the fiber-stacked samples exhibited higher hardness than those produced from powders. As shown in Fig. 2(c), this is visually evident by the dominance of warmer colors in the maps of the fiber-based samples. This difference is attributed to the sample microstructure thus fiber stacking appears to promote greater densification and a more compact matrix, which enhances mechanical strength.

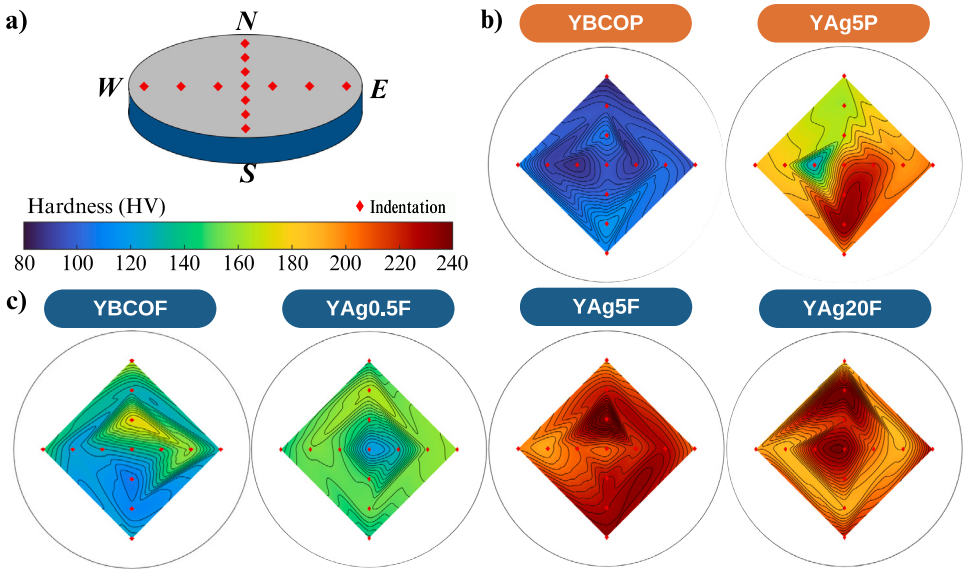

Fig. 2. (a) Schematic representation of the indentation pattern applied to the surface of the pellets. (b) Vickers hardness (HV) distribution maps for the YBCOP and YAg5P samples (compacted from powders). The color bar represents the hardness scale. (c) Vickers hardness (HV) distribution maps for the YBCOF, YAg0.5F, YAg5F, and YAg20F samples (compacted from fibers). (For interpretation of the references to color in this figure legend, the reader is referred to the web version of this article.)

The micrographs of the fracture surface (Fig. 3) reveal that the fiber-based samples exhibit a plate-like morphology with minimal intergranular voids, indicating a denser and more homogeneous structure. However, despite the higher hardness values, large cracks perpendicular to the main axis of the pellet developed after the heat treatments, as evidenced by the inset in Fig. 3.

In contrast, the powder-compacted samples exhibit a predominantly granular morphology with more significant porosity, although some plate-like regions are also present. This explains the hardness heterogeneity observed in the color maps in Fig. 2(a).

Beyond shaping methodology, silver addition also directly influenced sample hardness, consistent with literature reports [9–13]. Analysis of Fig. 2(b) and (c) reveals that, for a given shaping route, increasing Ag content in the ceramic matrix enhances hardness, as indicated by more intense red tones in the maps.

However, an analysis of hardness versus silver concentration (Fig. 4) reveals that this mechanical improvement reaches a limit. Hardness increases up to a concentration of 5 wt% Ag, beyond which no further significant gain is observed. This plateau, highlighted by the trend line, suggests a saturation of reinforcing effect as a consequence of silver addition.

Importantly, the hardness values were obtained from 13 measurements per sample to ensure a representative evaluation of material irregularity. The use of boxplots allows visualization of not only the median but also the data spread and outliers. To better interpret central tendency, a smoothed curve using piecewise cubic Hermite interpolation (PCHIP) was superimposed, preventing non-physical oscillations and clearly revealing the saturation behavior.

For a direct quantitative comparison, the hardness medians for each sample are listed in Table 1. The median was chosen as it is a robust central tendency measure, less sensitive to outliers.

Analysis of Table 1 shows that the reference sample YBCOF has 35% higher hardness than YBCOP, reinforcing the effectiveness of fiber stacking. The comparison between YAg5F and YAg5P reveals a 11% difference, indicating that the shaping methodology retains its influence even in the presence of silver. The synergistic effect of both factors is most evident when comparing YAg5F to the general reference YBCOP. The hardness increase reaches 125%, highlighting that the optimal combination of 5 wt% Ag and fiber shaping is key to improving mechanical strength. It is worth noting that all samples were pressed under identical time and pressure conditions, ensuring similar initial compactness. Thus, the observed effects can confidently be attributed to the processing route (powder vs. fiber) and silver concentration.

Table 1
Median standard deviation (SD) Vickers hardness values (in GPa) for samples formed from fibers (YBCOF, YAg0.5F, YAg5F, YAg20F) and from powder (YBCOP, YAg5P) with varying silver concentrations. Values correspond to the medians of the distributions shown in Fig. 4.

Sample	Hardness (GPa)
YBCOP	0.949 ± 0.095
YAg5P	1.932 ± 0.315
YBCOF	1.285 ± 0.198
YAg0.5F	1.451 ± 0.115
YAg5F	2.138 ± 0.175
YAg20F	2.109 ± 0.209

To clarify the origin of hardness heterogeneity and confirm silver distribution, energy-dispersive X-ray spectroscopy (EDS) analyses were performed. Elemental maps (Fig. 5) confirmed a notably homogeneous silver distribution in all formulations, with no evidence of large-scale clusters. This uniform silver distribution represents a significant advantage of the one-pot synthesis route, as it allows for a more direct evaluation of silver's intrinsic role in modifying YBCO's properties. This contrasts with traditional solid-state routes where, as reported in the literature [11,27,28], silver tends to localize in pores and form micrometric agglomerates. Consequently, the observed hardness variations can be more confidently attributed to microstructural changes (e.g., plate-like morphology and densification) rather than local fluctuations in silver concentration.

X-ray diffraction (XRD) analyses were performed to verify the phase purity of the samples. The diffractograms (Fig. 6(a)) reveal that the $YBa_2Cu_3O_{7-\delta}$ phase is the predominant component in all samples. For the silver-containing pellets, additional diffraction peaks corresponding to face-centered cubic (fcc) silver are observed at 2θ values of approximately 38.1° (111) and 44.5° (200).

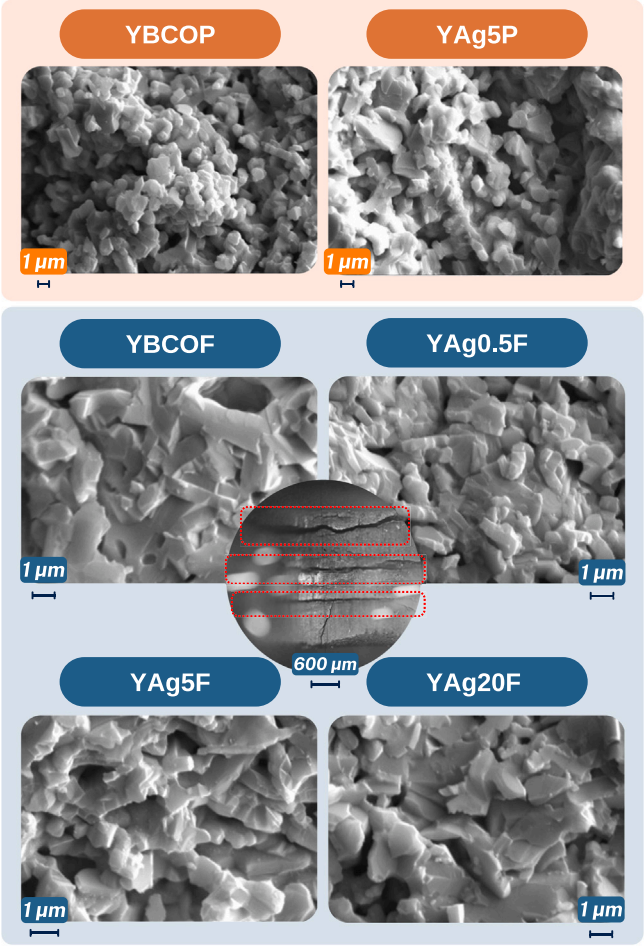

Fig. 3. Scanning electron microscopy (SEM) micrographs of the fracture surfaces of pellets compacted from powders (top row: YBCOP and YAg5P) and stacked nanofiber mats (bottom row: YBCOF, YAg0.5F, YAg5F, and YAg20F). The SEM images include a 1 μm scale bar. The inset shows an optical microscopy image of a crack perpendicular to the main axis in a fiber-based sample, highlighted by red lines; the inset scale bar corresponds to 600 μm.

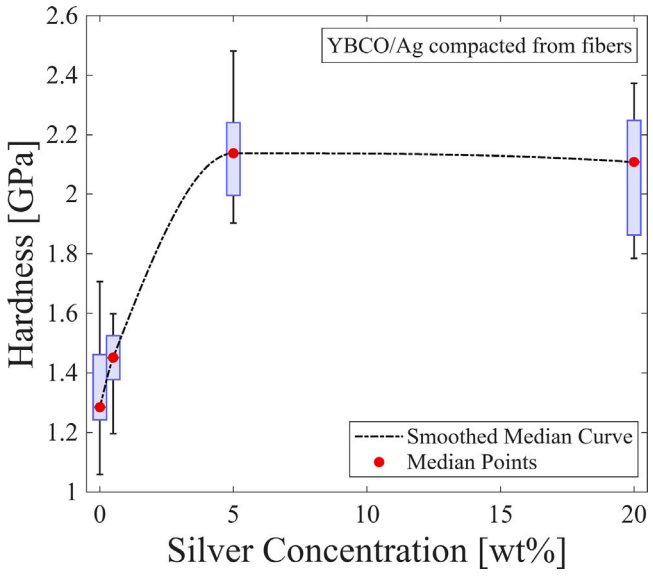

Fig. 4. Boxplot representation of hardness measurements for fiber-based YBCO samples with different silver contents (0.5, 5, and 20 wt%). The data were obtained from 13 indentations across the surface of each pellet. Each box summarizes the statistical distribution of hardness values (median, interquartile range, and overall spread). The black smoothed curve represents the trend of the median hardness as a function of Ag content. An increase in hardness is observed up to 5 wt% Ag, followed by a plateau at higher concentrations.

A key finding from the XRD analysis is the progressive broadening of diffraction peaks with increasing silver concentration, especially in the regions 45–49° (Fig. 6(b)) and 57–60° (Fig. 6(c)). This broadening is inversely related to the coherent diffraction domain size, suggesting that silver addition refines the microstructure. To quantify this effect, the average crystallite size (D) was estimated from XRD peak broadening (Eq. (1)) as described in the methodology section, considering the FWHM and Bragg angle (θ) of the eleven most intense diffraction peaks. It is important to note that the crystallite size estimated from XRD corresponds to the coherent diffraction domain size and should not be directly interpreted as the grain size observed in SEM images.

Results indicate a systematic decrease in crystallite size with increasing silver content (e.g., from (30.11 ± 0.17) nm in YBCOF to (25.00 ± 0.43) nm in YAg20F), as shown in Fig. 6d. This reduction in crystallite size suggests that silver incorporation influences the nucleation and growth mechanisms during synthesis, leading to a refined microstructure. This silver-induced microstructural modification strongly affects superconducting properties, as grain boundary density and domain coherence govern current transport and flux pinning [6,18].

Superconducting properties were initially investigated via magnetization versus temperature (M-T) curves (Fig. 7). All samples show a clear superconducting transition with critical temperatures (T_c) around 92 K. The YAg5F sample exhibits the strongest diamagnetic signal (Meissner effect) in the zero-field-cooled (ZFC) curve, indicating a large superconducting volume fraction, which is a prerequisite for high critical current density.

Magnetic flux pinning capability, crucial for practical applications, was assessed by the difference between FC and ZFC curves ($\Delta M = M_{FC} - M_{ZFC}$) (Fig. 8). YAg5F shows the highest ΔM, suggesting the most effective pinning among fiber samples. Interestingly, YBCOP (powder without silver) exhibits stronger pinning than YBCOF (fiber without silver), likely due to its granular morphology (Fig. 3), which offers a higher density of grain boundaries acting as extrinsic pinning centers.

The critical current density J_c, the most relevant property for transport applications, was determined from magnetic hysteresis (M-H) loops. The loop width is directly proportional to J_c, see Eq. (2). As expected, YAg5F exhibits the largest hysteresis area, corroborating the M–T results. The calculated $J_c(H)$ curves confirm that the 5 wt% silver samples (YAg5F and YAg5P) exhibit the best performance (Fig. 9), with values of approximately 6×10^3 A cm^{-2} and 4.8×10^3 A cm^{-2} at 4.2 K, respectively.

The reference materials YBCOP and YBCOF exhibited J_c values of 3.2×10^3 A cm^{-2} and 2.5×10^3 A cm^{-2} at 4.2 K, respectively. Although these values do not represent the highest J_c reported for polycrystalline YBCO [19–21], they are comparable to results obtained via chemical routes, which are more directly related to the synthesis approach adopted in this work, typically reaching up to ~5.0×10^3 A cm^{-2} under similar conditions [20].

At 77 K, the J_c obtained for YBCOP (2.3×10^2 A cm^{-2}) exceeds that reported on the literature for pure granular YBCO (1.6×10^2 A cm^{-2}) [19], while YBCOF exhibits a J_c that is only 12.5% greater than the reference value, i.e., 1.8×10^2 A cm^{-2}).

The enhancement of J_c at 5 wt% silver is followed by a degradation at higher concentrations, such as 20 wt%, where a value of 2.3×10^3 A

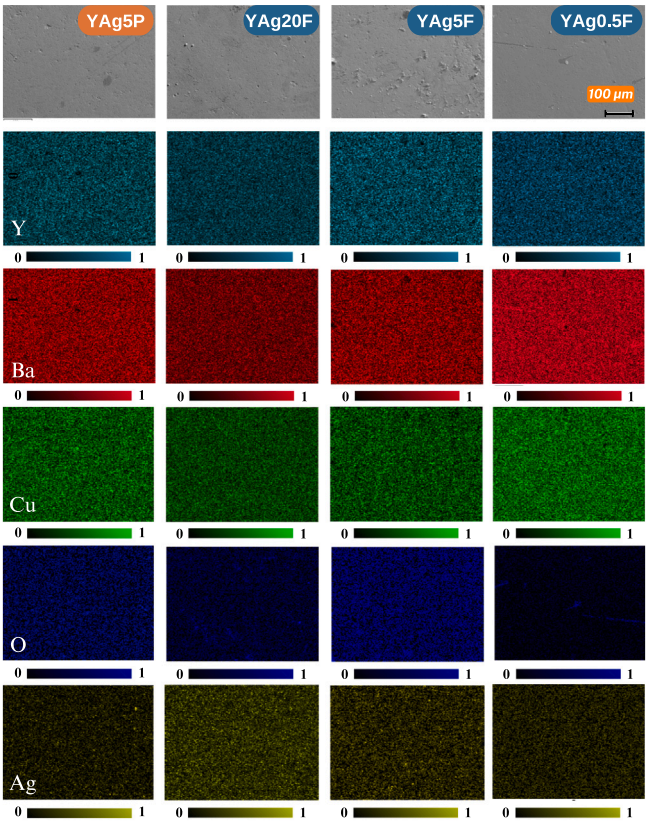

Fig. 5. Elemental distribution maps obtained by energy-dispersive X-ray spectroscopy (EDS), together with the corresponding polished surface images, for the YAg0.5F, YAg5F, YAg20F (fiber-based), and YAg5P (powder-based) pellets. The maps show the spatial distribution of Y, Ba, Cu, O, and Ag, highlighting the homogeneous dispersion of silver within the YBCO ceramic matrix. The scale bar corresponds to 100 μm. Elemental distributions are represented using a relative intensity scale (0–1), where brighter regions indicate higher elemental concentration and darker regions indicate lower concentration.

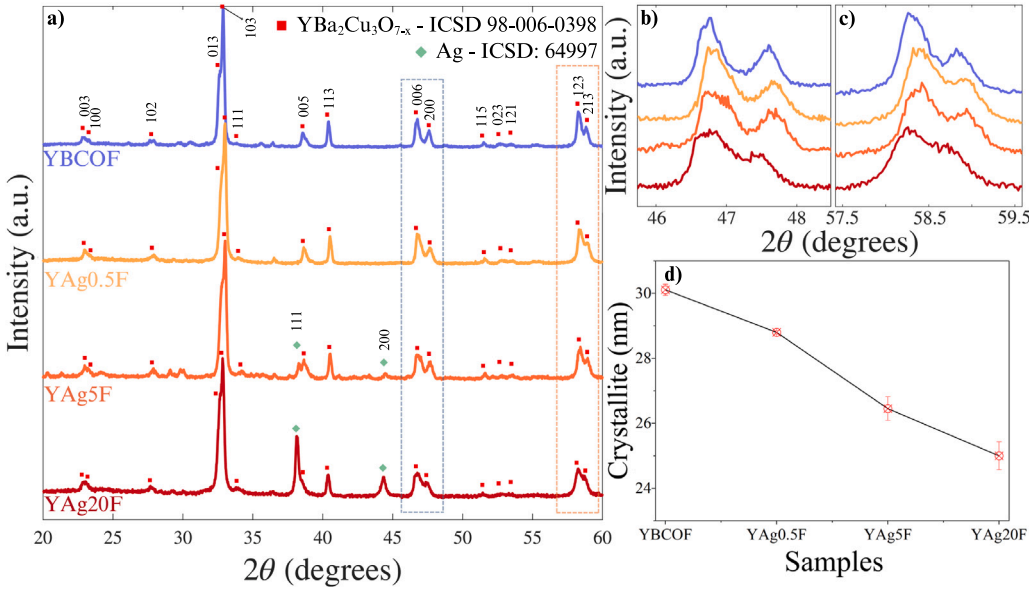

Fig. 6. X-ray diffraction (XRD) patterns of YBCOF, YAg0.5F, YAg5F, and YAg20F samples are shown in panel (a), where $YBa_2Cu_3O_{7-\delta}$ is identified as the major phase. The reference patterns for YBCO and metallic Ag are also included, along with the indexed (hkl) planes. Panels (b) and (c) present magnified views of selected diffraction regions, highlighting the progressive peak broadening with increasing silver concentration, particularly in the 2θ ranges of 45–49° and 57–60°. Panel (d) shows the average crystallite size (nm), estimated from peak broadening using the Scherrer equation, with error bars representing measurement uncertainties. The observed peak broadening suggests a reduction in crystallite size with increasing Ag content.

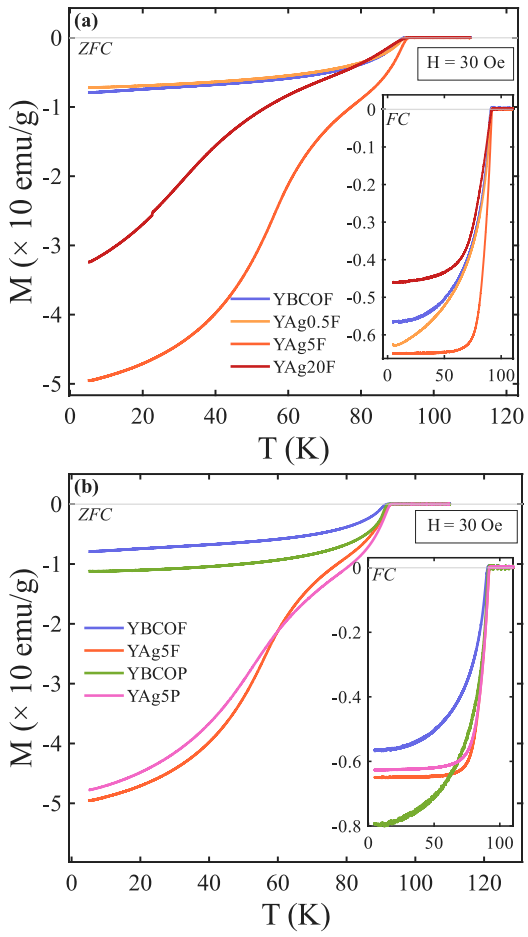

Fig. 7. Analysis of the superconducting properties of YBCO-based samples prepared by different routes. The effect of silver concentration is shown for fiber-compacted samples (YBCOF, YAg0.5F, YAg5F, and YAg20F) under (a) Zero-Field-Cooled (ZFC) and Field-Cooling (FC) protocols. A comparison of compaction methodologies is presented in panels (b), which display the ZFC and FC curves for powder-based samples (YBCOP, YAg5P) alongside their fiber-based counterparts (YBCOF, YAg5F). The measurements were conducted under an applied magnetic field of 30 Oe.

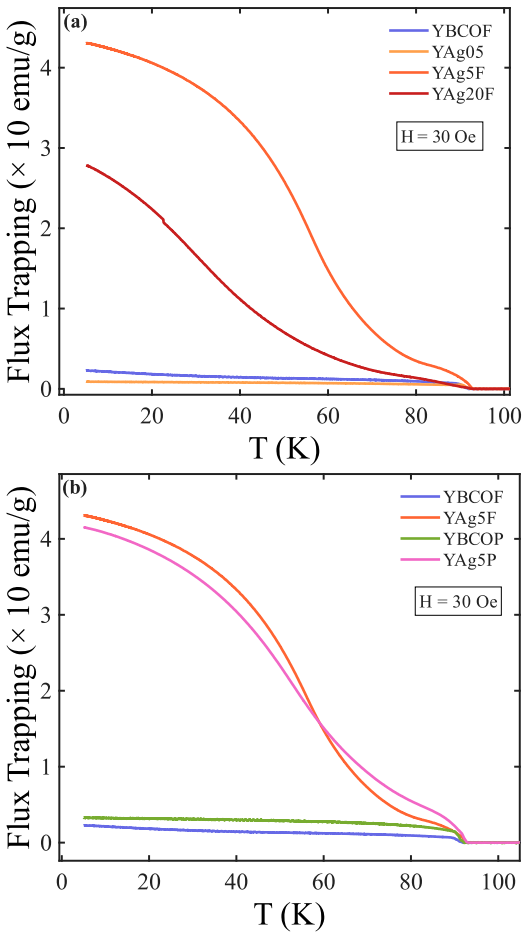

Fig. 8. Temperature dependence of the trapped magnetic flux for YBCO and YBCO/Ag samples, indicating their flux pinning performance. (a) Trapped flux as a function of silver content for fiber-compacted samples (YBCOF, YAg0.5F, YAg5F, and YAg20F). (b) The influence of the compaction methodology is shown by comparing samples made from powder (YBCOP, YAg5P) and fibers (YBCOF, YAg5F). All samples were field-cooled in 30 Oe to induce flux trapping.

cm^{-2} is observed, reflects the competing effects of silver incorporation and grain boundary interactions in the YBCO microstructure [18]. On one hand, grain boundaries act as effective flux pinning centers, which is beneficial for J_c. Higher densities of structural defects and interfaces may enhance vortex pinning. XRD results indicate that silver addition progressively reduces the coherent diffraction domain size, suggesting a refinement of the microstructure. On the other hand, grain boundaries in YBCO may act as weak links, potentially hindering supercurrent flow.

At an optimal concentration (5 wt%), the presence of silver appears to enhance flux pinning without significantly compromising intergranular current flow. In Ref. [18], a similar behavior was attributed to the formation of ideal superconductor/normal/superconductor (S/N/S) Josephson junctions at the grain boundaries in the presence of silver. Following this interpretation, the YAg5F sample — characterized by an intermediate crystallite size — thus represents a near-optimal balance between these competing effects.

In contrast, at 20 wt% silver, the detrimental effects appear to dominate. Even though the coherent diffraction domain size decreases further (25.00 ± 0.43 nm), the higher silver content likely increases the fraction of metallic normal regions within the ceramic matrix, in agreement with the interpretation proposed in Ref. [18]. Such regions may weaken the Josephson coupling between superconducting grains, partially decoupling them and drastically reducing the network's J_c. Therefore, according to our hypothesis, the degraded performance at 20 wt% Ag is not due to a lack of pinning centers, but rather to a dominant loss of intergranular connectivity. This highlights that controlling silver concentration is critical to achieving a delicate balance between enhancing intragrain pinning and preserving the essential intergrain current pathways in polycrystalline YBCO ceramics.

4. Conclusions

In this work, a synergistic strategy was explored to enhance the performance of YBCO/Ag superconducting composites by combining an one-pot synthesis route with an innovative shaping approach based on the stacking of ceramic fibers produced via SBS. The results clearly demonstrate the superiority of this route compared to conventional powder compaction. The denser, lamellar microstructure obtained from the stacked fibers led to a 35% increase in the mechanical hardness of pure YBCO. The incorporation of silver further improved the overall performance, with the 5 wt% Ag composition emerging as the optimal condition, achieving a remarkable 125% enhancement in hardness,

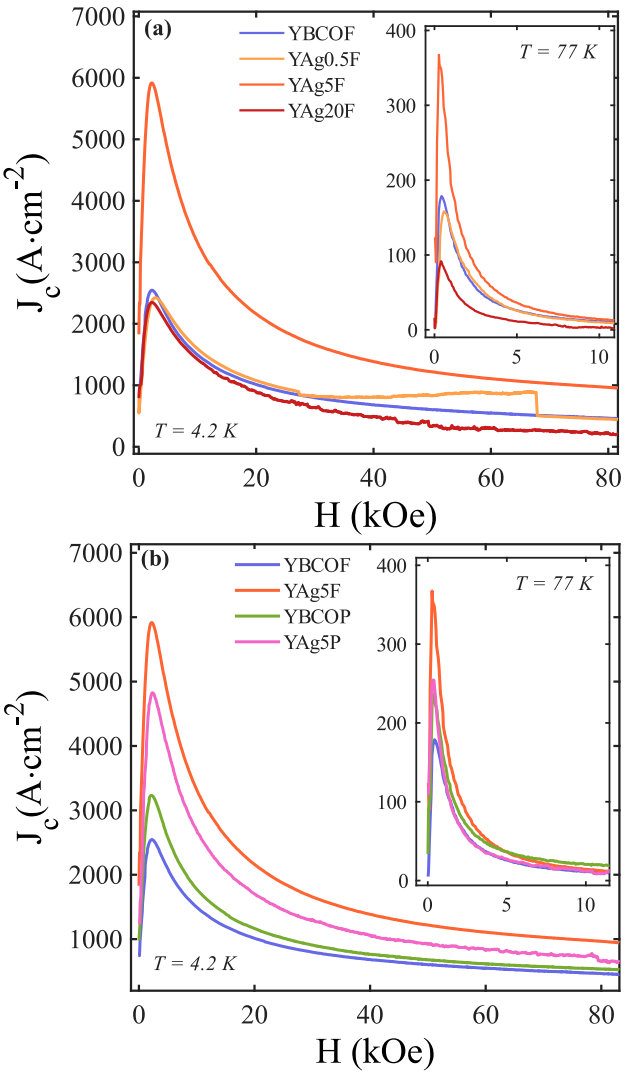

Fig. 9. Dependence of the critical current density $J_c(H)$ as a function of the applied magnetic field (H) for various YBCO samples, measured at 4, 2 K and 77 K. (a) J_c(H) curves for fiber-compacted samples with different Ag. (b) A comparison of the $J_c(H)$ curves of YBCO samples compacted from powders with those of fiber-compacted YBCO samples under an applied magnetic field (H).

although the samples densified from the fibers presented cracks perpendicular to the main axis following the heat treatment, and the highest J_c among all samples.

The optimal behavior observed at 5 wt% Ag is attributed to a critical balance between two competing mechanisms. On one hand, the homogeneously distributed silver, ensured by the one-pot synthesis, promotes microstructural refinement by reducing the crystallite size and promotes microstructural refinement and enhances flux pinning. On the other hand, excessive silver content (20 wt%) leads to the formation of thick metallic barriers at grain boundaries, suppressing intergranular Josephson coupling and severely reducing the electrical connectivity of the superconducting network. The YAg5F sample therefore represents an ideal balance point where flux pinning is maximized without significant loss of connectivity.

Overall, this study not only clarifies the multifaceted role of silver in YBCO-based composites but also establishes a promising processing route for fabricating superconducting materials with improved mechanical robustness. The combination of one-pot synthesis and fiber-based shaping enabled a homogeneous distribution of silver within the ceramic matrix, promoting simultaneous improvements in densification, hardness, and superconducting performance under optimal conditions. Beyond superconductivity, these findings highlight the broader potential of controlled metallic-phase incorporation as a strategy for tailoring the microstructure and multifunctional properties of advanced ceramic composites. The ability to engineer dense and mechanically robust ceramic architectures through fiber assembly may also open new perspectives for structural and functional ceramic systems requiring enhanced interfacial control and mechanical reliability. Future studies may focus on optimizing the SBS parameters to enhance fiber alignment, as well as extending this methodology toward the fabrication of superconducting wires, tapes, and other advanced ceramic-based devices for large-scale applications.

CRediT authorship contribution statement

Matheus P. Brambilla: Writing – original draft, Validation, Resources, Methodology, Investigation, Formal analysis, Data curation, Conceptualization. **Edimar A.S. Duran:** Writing – review & editing, Validation, Resources, Formal analysis, Data curation, Conceptualization. **Alfonso Pulgar:** Writing – review & editing, Validation, Resources, Formal analysis, Data curation, Conceptualization. **Maycon Motta:** Writing – review & editing, Visualization, Investigation, Formal analysis, Data curation. **Lucas B.S. da Silva:** Writing – review & editing, Visualization, Investigation, Formal analysis, Data curation. **Vasily S. Stolyarov:** Writing – review & editing, Visualization, Investigation, Formal analysis, Data curation. **Rodolfo Izquierdo:** Writing – review & editing, Visualization, Investigation, Formal analysis, Data curation. **Rafael Zadorosny:** Writing – review & editing, Visualization, Supervision, Resources, Project administration, Funding acquisition, Conceptualization. **Durval Rodrigues Jr:** Writing – review & editing, Visualization, Investigation, Formal analysis, Data curation.

Declaration of competing interest

The authors declare that they have no known competing financial interests or personal relationships that could have appeared to influence the work reported in this paper.

Acknowledgments

The author thanks the Brazilian agencies São Paulo Research Foundation FAPESP, grants 2022/12085-0, 2022/03124-1, and 2024/21097-7. This study was financed in part by the Coordenação de Aperfeiçoamento de Pessoal de Nível Superior - Brasil (CAPES) - Finance Code 001, and the support of the INCT project Advanced Quantum Materials, involving the Brazilian agencies CNPq (Proc. 408766/2024-7 and 150145/2026-8), FAPESP and CAPES, and CNPq (grants 302786/2025-2 and 310514/2025-8). We also acknowledge the Grupo de Polímeros (GPol) for their availability and support in the XRD analysis.

References

[1] M.-K. Wu, J.R. Ashburn, C. Torng, P.-H. Hor, R.L. Meng, L. Gao, Z.J. Huang, Y. Wang, a. Chu, Superconductivity at 93 K in a new mixed-phase Y-Ba-Cu-O compound system at ambient pressure, Phys. Rev. Lett. 58 (9) (1987) 908.

[2] S. Nishijima, S. Eckroad, A. Marian, K. Choi, W.S. Kim, M. Terai, Z. Deng, J. Zheng, J. Wang, K. Umemoto, et al., Superconductivity and the environment: A roadmap, Supercond. Sci. Technol. 26 (11) (2013) 113001.

[3] D. Wollman, D. Van Harlingen, W. Lee, D. Ginsberg, A. Leggett, Experimental determination of the superconducting pairing state in YBCO from the phase coherence of YBCO-Pb dc SQUIDs, Phys. Rev. Lett. 71 (13) (1993) 2134.

[4] A.K. Jha, K. Matsumoto, T. Horide, S. Saini, P. Mele, A. Ichinose, Y. Yoshida, S. Awaji, Controlling the critical current anisotropy of YBCO superconducting films by incorporating hybrid artificial pinning centers, IEEE Trans. Appl. Supercond. 26 (3) (2016) 1–4.

[5] E. Stepantsov, Anisotropy of high-temperature superconductivity in the (100) plane of YBa2Cu3O7 film, Crystallogr. Rep. 67 (3) (2022) 436–440.

[6] J.P. Singh, H. Leu, R.B. Poeppel, E. Van Voorhees, G. Goudey, K. Winsley, D. Shi, Effect of silver and silver oxide additions on the mechanical and superconducting properties of YBa2Cu3O7- δ superconductors, J. Appl. Phys. 66 (7) (1989) 3154–3159.

[7] D. Larbalestier, A. Gurevich, D.M. Feldmann, A. Polyanskii, High-T c superconducting materials for electric power applications, Nature 414 (6861) (2001) 368–377.

[8] D.K. Namburi, Y. Shi, D.A. Cardwell, The processing and properties of bulk (RE) BCO high temperature superconductors: current status and future perspectives, Supercond. Sci. Technol. 34 (5) (2021) 053002.

[9] P. Diko, G. Fuchs, G. Krabbes, Influence of silver addition on cracking in melt-grown YBCO, Phys. C: Supercond. 363 (1) (2001) 60–66.

[10] E. Mogilko, Y. Schlesinger, The route to the YBCO/Ag composite: structural and electrical properties, Supercond. Sci. Technol. 10 (3) (1997) 134.

[11] J.V. Congreve, Y. Shi, K.Y. Huang, A. Dennis, J.H. Durrell, D.A. Cardwell, Improving mechanical strength of YBCO bulk superconductors by addition of Ag, IEEE Trans. Appl. Supercond. 29 (5) (2019) 1–5.

[12] N.D. Kumar, P.M.S. Raju, S.P.K. Naik, T. Rajasekharan, V. Seshubai, Effect of Ag addition on the microstructures and superconducting properties of bulk YBCO fabricated by directionally solidified preform optimized infiltration growth process, Phys. C: Supercond. Appl. 496 (2014) 18–22.

[13] J. Baumann, Y. Shi, J.V. Congreve, J.H. Durrell, D.A. Cardwell, Statistical evaluation of the mechanical properties of partially oxygenated YBCO, oxygenated YBCO and oxygenated YBCO (Ag) single grains, Ceram. Int. 49 (19) (2023) 31734–31743.

[14] P.d. Azambuja, P. Rodrigues Júnior, A.R. Jurelo, F.C. Serbena, C.E. Foerster, R.M. Costa, G.B.d. Souza, C.M. Lepienski, A.L. Chinelatto, Effects of Ag addition on some physical properties of granular YBa2Cu3O7-δ superconductor, Braz. J. Phys. 39 (2009) 638–644.

[15] B.A. Malik, M.A. Malik, K. Asokan, Magneto transport study of YBCO: Ag composites, Curr. Appl. Phys. 16 (10) (2016) 1270–1276.

[16] B. Dwir, D. Pavuna, M. Affronte, H. Berger, J. Tholence, Percolation and electronic properties of superconducting (YBa 2 Cu 3 O 7- δ) 1- x Ag x ceramics and thick films, J. Supercond. 2 (1989) 419–426.

[17] Y. Nishi, S. Moriya, S. Tokunaga, T c increase with Ag addition in the 596-1596-1596-1system, J. Mater. Sci. Lett. 7 (1988) 596–598.

[18] A. Harabor, P. Rotaru, N.A. Harabor, P. Nozar, A. Rotaru, Structural, thermal and superconducting properties of Ag2O-doped YBa2Cu3O7-x composite materials, Ceram. Int. 49 (9) (2023) 14904–14916.

[19] F. Zhao, B. Zhang, X. Su, Y. Zhao, X. Zhang, Mechanism of solid solution-driven texture induced by Ag doping in YBCO superconductor, Adv. Sci. (2026) e22923.

[20] D. Zhang, C. Boffo, D.C. Dunand, Additively-manufactured monocrystalline YBCO superconductor, Nat. Commun. 16 (1) (2025) 1933.

[21] F. Yu, R.P. Thedford, T.A. Tartaglia, S.S. Sheth, G. Freychet, W.R. Tait, P.A. Beaucage, W.L. Moore, Y. Li, J.G. Werner, et al., Hierarchically ordered porous transition metal compounds from one-pot type 3D printing approaches, Nat. Commun. 16 (1) (2025) 7704.

[22] M. Rotta, M. Motta, A.L. Pessoa, C.L. Carvalho, C.V. Deimling, P.N. Lisboa-Filho, W.A. Ortiz, R. Zadorosny, One-pot-like facile synthesis of YBa2Cu3O7-δ superconducting ceramic: Using PVP to obtain a precursor solution in two steps, Mater. Chem. Phys. 243 (2020) 122607.

[23] M. Rotta, L. Zadorosny, C. Carvalho, J. Malmonge, L. Malmonge, R. Zadorosny, YBCO ceramic nanofibers obtained by the new technique of solution blow spinning, Ceram. Int. 42 (14) (2016) 16230–16234.

[24] A. Pessoa, M. Raine, D. Hampshire, D. Namburi, J. Durrell, R. Zadorosny, Successful production of solution blow spun YBCO+ Ag complex ceramics, Ceram. Int. 46 (15) (2020) 24097–24101.

[25] D.-X. Chen, R.B. Goldfarb, Kim model for magnetization of type-II superconductors, J. Appl. Phys. 66 (6) (1989) 2489–2500.

[26] C. Bean, M.V. Doyle, A. Pincus, Synthetic high-field, high-current superconductor, Phys. Rev. Lett. 9 (3) (1962) 93.

[27] T. Nishio, Y. Itoh, F. Ogasawara, M. Suganuma, Y. Yamada, U. Mizutani, Superconducting and mechanical properties of YBCO-Ag composite superconductors, J. Mater. Sci. 24 (1989) 3228–3234.

[28] W. Tuan, J. Wu, Effect of microstructure on the hardness and fracture toughness of YBa 2 Cu 3 O 7- x/Ag composites, J. Mater. Sci. 28 (1993) 1415–1420.